Earth and Planetary Science Letters 619 (2023) 118325

Contents lists available at ScienceDirect

Earth and Planetary Science Letters

journal homepage: www.elsevier.com/locate/epsl

Satellite derived SO_2 emissions from the relatively low-intensity, effusive 2021 eruption of Fagradalsfjall, Iceland

Ben Esse [a,*], Mike Burton [a], Catherine Hayer [a,b], Melissa Anne Pfeffer [c], Sara Barsotti [c], Nicolas Theys [d], Talfan Barnie [c], Manuel Titos [e]

[a] Department of Earth and Environmental Sciences, The University of Manchester, Manchester, UK
[b] HAMTEC for EUMETSAT, Darmstadt, Germany
[c] Icelandic Meteorological Office, IS-150 Reykjavík, Iceland
[d] Royal Belgian Institute for Space Aeronomy, Brussels, Belgium
[e] University of Granada, Granada, Spain

ARTICLE INFO

Article history:
Received 29 March 2023
Received in revised form 17 July 2023
Accepted 22 July 2023
Available online 8 August 2023
Editor: C.M. Petrone

Dataset link: https://distributions.aeronomie.be/

Dataset link: https://www.ready.noaa.gov/data/archives/gfs0p25/

Dataset link: https://www.doi.org/10.6084/m9.figshare.22303435

Keywords:
volcanology
sulphur dioxide
TROPOMI
Fagradalsfjall
volcano monitoring

ABSTRACT

In March 2021 an effusive eruption began at the Fagradalsfjall volcanic system in Iceland, ending nearly 800 years of dormancy on the Reykjanes peninsula. The eruption produced lava flows and moderate gas emissions and, although it did not cause significant disruption, highlighted the need for near real-time monitoring of volcanic activity on the peninsula for future eruptions. The activity passed through several phases, each characterised by a different eruption style, providing a rich testbed for monitoring methodologies.

We present measurements of the volcanic sulphur dioxide (SO_2) emission rate and injection altitude throughout the eruption, generated by combining satellite SO_2 imagery from TROPOMI with PlumeTraj, a back-trajectory analysis toolkit. We compare the results with ground-based measurements of the emission rate and plume altitude, finding excellent agreement in the plume altitude. Reasonable agreement was also found between the measured emission rates, with the best match for stronger and more continuous emissions. This demonstrates the ability for PlumeTraj to monitor SO_2 emissions from future effusive eruptions, while highlighting the need for care when analysing results from low altitude plumes or during periods of high cloud cover.

1. Introduction

On 19th March 2021 an effusive eruption began at Fagradalsfjall on the Reykjanes Peninsula in Iceland (Global Volcanism Program, 2021; Óladóttir, 2022). The eruption marked the end of 781 years of dormancy on the peninsula and lasted six months, ending on 18th September (Barsotti et al., 2023). Assessment of the post-glacial lavas on the peninsula show three periods of episodic volcanic activity in the last 4000 years, each separated by approximately 800 years and lasting roughly 200-400 years (Sæmundsson et al., 2020). The eruption produced lava and gas emissions, and led to the creation of a lava field filling the nearby valleys (Pedersen et al., 2022a). Effusive eruptions such as this are typically lower risk than explosive ones, however there is still a strong requirement to monitor them closely. Lava flows can damage or destroy houses and infrastructure depending on the location of the eruption, and gas emissions can significantly impact local air quality (Thordarson and Self, 2003). The Reykjanes Peninsula is home to 70% of Iceland's population (including Iceland's capital city, Reykjavík) and is the location of the Svartsengi and Reykjanes geothermal power plants and Keflavík international airport (Tarquini et al., 2020). Fortunately, this eruption did not damage any infrastructure, however it did highlight the potential disruption future activity in the Peninsula could cause (Pedersen et al., 2022b).

For these reasons, monitoring of volcanic activity in the Reykjanes Peninsula is of critical importance, both before and during eruptions. Eruption precursors can help to identify the time and location of the onset of an eruption, while monitoring activity in near real-time can help to inform any disaster response to mitigate risks from volcanic hazards, as well as help to forecast changes

* Corresponding author.
E-mail address: benjamin.esse@manchester.ac.uk (B. Esse).

https://doi.org/10.1016/j.epsl.2023.118325

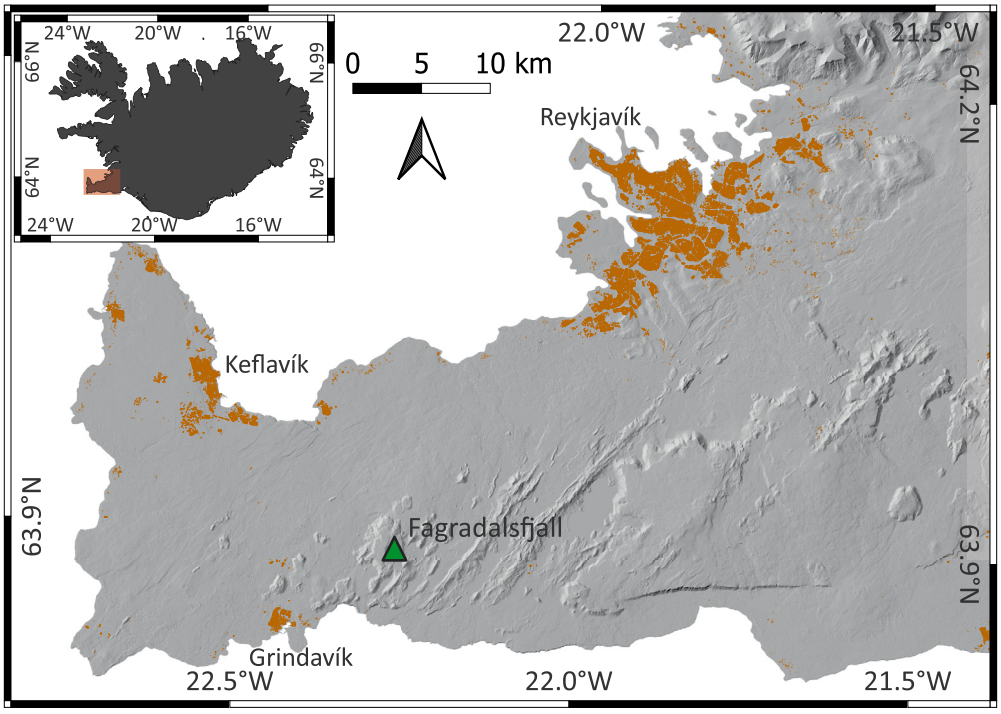

Fig. 1. Map of Iceland (inset map) with a zoomed map of the Reykjanes Peninsula (main map). Populated areas are marked in orange and the location of the vents is given by the green triangle. Background topography is taken from ÍslandsDEM, v1.0 (https://atlas.lmi.is/mapview/?application=DEM, visited 08/09/2022) which was acquired prior to the unrest and eruption.

in future activity (Lowenstern et al., 2022; Pallister et al., 2019; Sparks, 2003).

Here we will focus on monitoring volcanic gas emissions, specifically sulphur dioxide (SO_2), using satellite remote sensing. Monitoring gas emissions is important as variations in their magnitude and composition reflect changes in the state of the magma supplying the volcano (Aiuppa et al., 2007; Oppenheimer et al., 2011; Salerno et al., 2018). Gas emissions can also pose a direct hazard by degrading air quality (Carlsen et al., 2021; Ilyinskaya et al., 2017; Tam et al., 2016; Whitty et al., 2020) and impacting local or even global climate (Robock, 2000; von Glasow et al., 2009), while knowing the rate and altitude of emissions is key to accurately forecast the dispersal of volcanic gas plumes (Barsotti, 2020; Barsotti et al., 2023; Kristiansen et al., 2010; Pfeffer et al., 2018).

Historically, it has been less common to use satellite sensors to monitor gas emissions from smaller effusive eruptions as the (typically) low altitude, low gas concentration, and small spatial extent of the plumes makes such measurements difficult (Hayer et al., 2016). However, recent advances in the satellite instruments and analysis routines are opening the door to global monitoring of weaker effusive gas emissions (Carn et al., 2017; Queißer et al., 2019; Theys et al., 2019, 2021). Satellites also provide continuous daily (or more frequent) measurements, making them useful for monitoring ongoing activity and capturing any changes in activity without the need for a dedicated ground-based monitoring network or continuous manual observations. This makes them ideal for monitoring difficult to access, remote or dangerous volcanoes, as well as for complementing ground-based measurements at already monitored volcanoes.

We present measurements of the SO_2 emissions from Fagradalsfjall throughout the 2021 eruption, using SO_2 imagery from the Tropospheric Monitoring Instrument (TROPOMI) onboard the European Space Agency's (ESA) Sentinel-5P satellite (Veefkind et al., 2012), generated using the Covariance-Based Retrieval Algorithm (COBRA) (Theys et al., 2021), an updated retrieval method that is more sensitive than the operational product. By combining this SO_2 imagery with the PlumeTraj back-trajectory analysis toolkit, we calculate time series of the emission rate and plume injection altitude, comparing with ground-based mobile Differential Optical Absorption Spectroscopy (mobileDOAS) and calibrated visible camera measurements, respectively. The PlumeTraj method has been applied to several eruptions previously, including Calbuco in Chile (Pardini et al., 2017), Whakaari in New Zealand (Burton et al., 2021), Piton de la Fournaise in La Réunion (Hayer et al., 2023), and La Soufrière in St. Vincent (Esse et al., 2023), as well as to passive degassing from Etna in Italy (Queißer et al., 2019). The application of PlumeTraj has so far been restricted to SO_2 emissions, however it could in theory be applied to any species emitted from a point source, including volcanic ash or other gases.

2. Eruption setting and overview

The Reykjanes Peninsula has a history of episodic volcanic eruptions, with the most recent before 2021 ending just under 800 years ago. The 2021 eruption was preceded by a period of intrusive activity on the Peninsula from December 2020 to February 2021, with increased seismicity and deformation (Barsotti et al., 2023; Flóvenz et al., 2022; Sigmundsson et al., 2022). Seismicity jumped again on 24th February 2021, increasing through March until the onset of the eruption within the Geldingadalir valley (63.905°N, 22.273°W), 4.7 km north of the coast, at 20:45 (local time) on 19th March (Fig. 1). The eruption was effusive, with lava flows creating a lava field around the vents and filling the nearby valleys. The eruption lasted until 18th September, progressing through distinct phases and sub-phases in activity (Barsotti et al., 2023; Pedersen et al., 2022a). A second eruption of the Fagradalsfjall volcanic system occurred from 3rd – 21st August 2022 in the Meradalir valley, adjacent to the Geldingadalir valley. A third began on 10th July 2023 just northwest of Litli Hrútur hill.

The eruption phases outlined by Barsotti et al. (2023) are summarised here for reference. The 2021 eruption started with low intensity activity (Phase 1, 19th March – 5th April) with stable lava

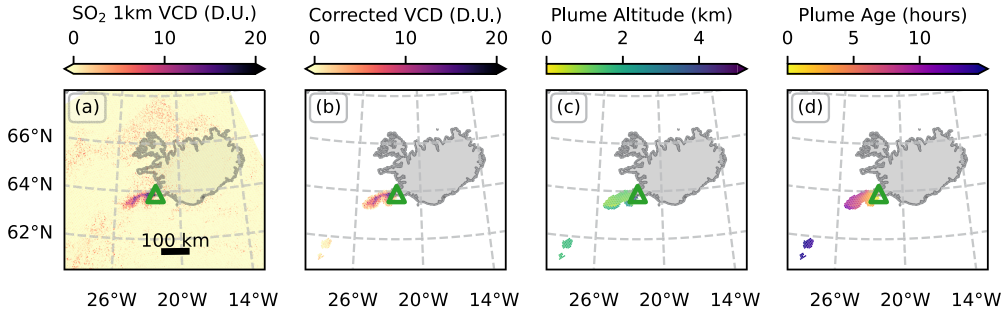

Fig. 2. PlumeTraj results for the plume measured on 2nd May 2021 (orbit number 18403), showing (a) the measured SO_2 VCD assuming a 1 km thick uniformly distributed plume, centred on 0.5 km above ground level, (b) the corrected VCD, (c) the plume altitude and (d) the plume age. The location of the vent is given by the green triangle.

emission and weak but detectable gas emissions. This continued through Phases 2a (5th – 14th April) and 2b (14th – 27th April) as additional eruptive fissures opened. In Phase 3a (27th April – 2nd May) the activity transitioned to stable lava fountaining, soon changing again to pulsating lava fountains (Phase 3b, 2nd – 11th May), with pulses in fountaining separated by a few minutes. Into Phase 3c (11th – 28th June) the fountaining was accompanied by sustained outpouring of lava. From 28th June the activity style changed again, with pauses in activity separating intense periods of activity (Phase 4a, 28th June – 2nd September). The pauses lasted several hours, to a maximum of roughly 35 hours. Phase 4b (2nd – 18th September) began with a 9 day pause in activity followed by a final week of eruption until the cessation of surface activity on 18th September.

Note that these are the same main phases outlined by Pedersen et al. (2022a), though there the authors identify subphase 4b as a separate Phase 5.

From visible observations the emitted gas plume was typically optically thin throughout the eruption (mostly faint and transparent). This was less so during Phase 3b when it was noted that the plumes were typically more condensed. The plume also tended to be more opaque in the presence of cold fronts, clouds and precipitation as it condensed more easily under these conditions.

Lavas from the eruption were also sampled throughout, providing a time-series in lava geochemistry through the phases of the eruption (Bindeman et al., 2022; Halldórsson et al., 2022). These revealed a rapid shift in the geochemistry of the erupted lava in the early phases of the eruption, reflecting a shift in the source from shallow ($<$ 8 km) to deeper depths ($\sim$19 km) throughout March and April, before plateauing from May onwards (Halldórsson et al., 2022). The same study also reports the gas chemistry of the plume measured by Open-Path Fourier Transform Infrared Spectroscopy (OP-FTIR) and using a MultiGas instrument between 20th March – 6th April, with values for the SO_2 content of the plume of 4.7 ($\pm$ 3.1) and 11 ($\pm$ 3) mol%, respectively. Both instruments also show the plume is dominated by H_2O and CO_2, with OP-FTIR also quantifying HCl and HF at 0.09 ($\pm$ 0.05) and 0.04 ($\pm$ 0.02) mol%, respectively (Halldórsson et al., 2022, supporting material).

3. Data and methods

3.1. Satellite SO_2 emission measurements

The satellite SO_2 imagery used in this study was taken by the TROPOMI instrument onboard ESA's Sentinel-5P satellite (S5P), which was launched in October 2017 (with scientific data available since May 2018). TROPOMI has a swath width of 2600 km and a spatial resolution of 5.5 x 3.5 km at nadir (along x across track, updated from 7.0 x 3.5 km in August 2019). For this study we chose to use the Covariance-Based Retrieval Algorithm (COBRA) product developed by Theys et al. (2021) as this retrieval offers a significant reduction in noise compared to the operational product. This is particularly useful when looking at weaker emissions low in the atmosphere, as with this eruption, however the plumes were still detectable with the operational product.

TROPOMI provides daily SO_2 imagery but does not contain key information on the altitude of the plume (required to calculate the mass of SO_2 in each pixel), nor the time or altitude of emission from the source, all of which are needed to reconstruct the SO_2 emission history. There are several ways to infer emission rates from satellite imagery (Theys et al., 2013), but here we use the PlumeTraj back-trajectory toolkit. PlumeTraj takes the SO_2 imagery from TROPOMI and tracks the plume back to the volcano to calculate the sub-daily SO_2 emission as a function of time and altitude. More details on PlumeTraj can be found in the supplementary material.

3.2. Ground-based measurements

We also present data taken by the Icelandic Meteorological Office (IMO) during the eruption as a comparison to the satellite results. MobileDOAS traverse measurements were taken to calculate an instantaneous SO_2 emission rate taken by performing car-based traverses of the plume downwind of the vent whenever possible throughout the eruption. More details on the traverse measurements can be found in the supplementary material and will be presented in detail in future publications. Plume altitude measurements were also made using visible cameras installed around the eruption site, calibrated to calculate the plume altitude when visible, providing plume bottom and top altitude estimates (Barnie et al., 2023; Barsotti et al., 2023). Finally, we include measurements of the time averaged lava discharge rate (TADR) calculated from photogrammetric surveys of the emitted lava flows and field (Pedersen et al., 2022a) in order to compare variations in lava effusion rate with measured SO_2 emissions.

4. Results

4.1. PlumeTraj results

TROPOMI was able to detect SO_2 plumes from Fagradalsfjall throughout the eruption. Analysis was attempted on each day from 19th March – 19th September (185 days). No emissions were detected on 27 days, including on the first day of the eruption (the overpass time on this day was before the onset of the eruption), during the pause in activity at the start of Phase 4b, and on the day after the eruption ended. No analysis was possible on 1st July due to there being no COBRA data available for this day. Fig. 2 shows an example of PlumeTraj results for a plume measured on 2nd May 2021 (chosen as an example for the overlap of PlumeTraj results with available traverse and plume altitude data).

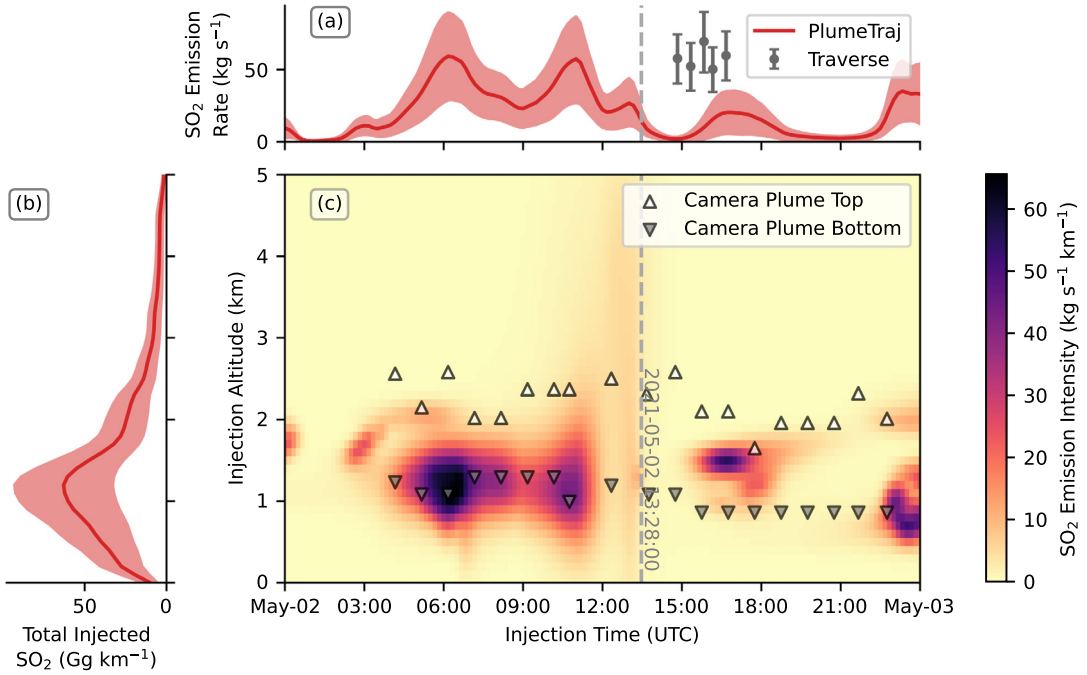

Fig. 3. Calculated SO_2 emissions for 2nd May 2021. Data comes from two orbits (numbers 18403 and 18417), with the overpass time of orbit 18403 on 2nd May marked by the grey dashed line. Subplots show (a) the time varying SO_2 emission rate from PlumeTraj (red line, shaded region gives uncertainty) with traverse measurements for comparison (grey points, bars give uncertainty), (b) the total mass of SO_2 injected as a function of altitude, and (c) the emission intensity as a function of both time and altitude, with plume top and bottom measurements from ground-based cameras (white and grey triangles).

With the plume altitude known, the SO_2 mass within each pixel is calculated and the full SO_2 emission history is generated using the injection time and altitudes. Fig. 3 shows the emissions measured on 2nd May, which includes the data shown in Fig. 2 as well as from the orbit measured on 3rd May (orbit number 18417). Also shown are the emission rates measured by mobileDOAS and plume heights from visible cameras (Barnie et al., 2023; Barsotti et al., 2023).

The SO_2 emission rate measured by PlumeTraj is variable but tends to decrease with plume age, reflecting the SO_2 dropping in concentration due to dispersal and chemical processing. This can be seen when comparing to the traverse emission rates. The emissions calculated just before the overpass time are from sections of the plume that are relatively young, and the emission rates are of the same magnitude as the traverses measured a few hours later. After the overpass, however, the plume pixels contributing to these emission rates are almost 24 hours old (measured at roughly 13:30 on 3rd May), and we see that the emission rates are much lower for the PlumeTraj results than for the traverses. Note that the smearing of the plume across a wide range of altitudes near to the overpass time is because trajectories from plume pixels so close to the vent do not have enough time to diverge sufficiently to provide an accurate altitude, resulting in a large uncertainty.

The PlumeTraj injection altitudes match very well with those measured on the ground. PlumeTraj does seem to track the plume bottom altitude more closely, though the cause of this is not certain. This could reflect some bias introduced by the coarse resolution digital elevation model used within GFS not reflecting the finer details of the true topography, the plume lowering in altitude slightly downwind after emission, or that the SO_2 is simply concentrated in the lower portion of the visible plume.

Fig. 4 shows the PlumeTraj results for the whole eruption, along with the mobileDOAS traverses, visible camera plume altitudes (Barnie et al., 2023; Barsotti et al., 2023) and lava TDAR (Pedersen et al., 2022a). Uncertainties on the peak emission rates from TROPOMI are taken from the uncertainty at the point in time at which the peak value was measured.

We highlight that the emission rates measured from Fagradalsfjall are relatively high compared to many degassing volcanoes. Carn et al. (2017) report effusive emissions from 0.4 – 85 $kg{\cdot}s^{-1}$, though this is achieved by stacking multiple satellite images to reduce the noise, not on daily SO_2 images as used here. However, the measured emission rates are still much lower than for many eruptions, including, for example, 200 $kg{\cdot}s^{-1}$ during the 2020 eruption of Piton de la Fournaise, Réunion, (Hayer et al., 2023), 1000 $kg{\cdot}s^{-1}$ during the 2014 – 2015 eruption of Holuhraun, Iceland, (Pfeffer et al., 2018), and ∼5000 $kg{\cdot}s^{-1}$ during the 2021 eruption of La Soufrière, St. Vincent, (Esse et al., 2023). Due to this, as well as the relatively low plume altitude and high cloud cover during this eruption, the PlumeTraj emission rates are likely to be underestimates, especially for parts of the plume that are older. We therefore took the peak SO_2 emission rate for each day to compare with the traverses as this is assumed to be the closest to the true emission rate. The time of the peak emission rate tended to be nearer to the overpass time (when the plume is young), though a range of plume age of peak emission was seen throughout, especially during the episodic behaviour (Fig. S1).

The PlumeTraj results are variable throughout the eruption, with low emission rates (10 – 20 $kg{\cdot}s^{-1}$) and low injections altitudes (< 1 km) during Phases 1 and 2. Both the emission rate and injection altitude increase through Phase 3a and into Phases 3b and 3c, with emission rates of 50 – 150 $kg{\cdot}s^{-1}$ and injection altitudes up to ∼4.5 km measured. Emission rates throughout June and through Phase 4a became roughly bimodal, with days of low emission (10 – 20 $kg{\cdot}s^{-1}$) and days of high emission (70 – 100 $kg{\cdot}s^{-1}$), reflecting the switch to more episodic activity. There are three distinct pulses in higher SO_2 emission seen, both in terms of emission rate and injection altitude, in May, June and mid-July to mid-August. These are separated by periods of weaker (or even undetectable) emission and lower plume altitudes.

No emissions are seen during the pause in activity at the beginning of Phase 4b, with weak emissions seen after activity recommenced until the end of the eruption. No further SO_2 emissions were detected after the end of the eruption.

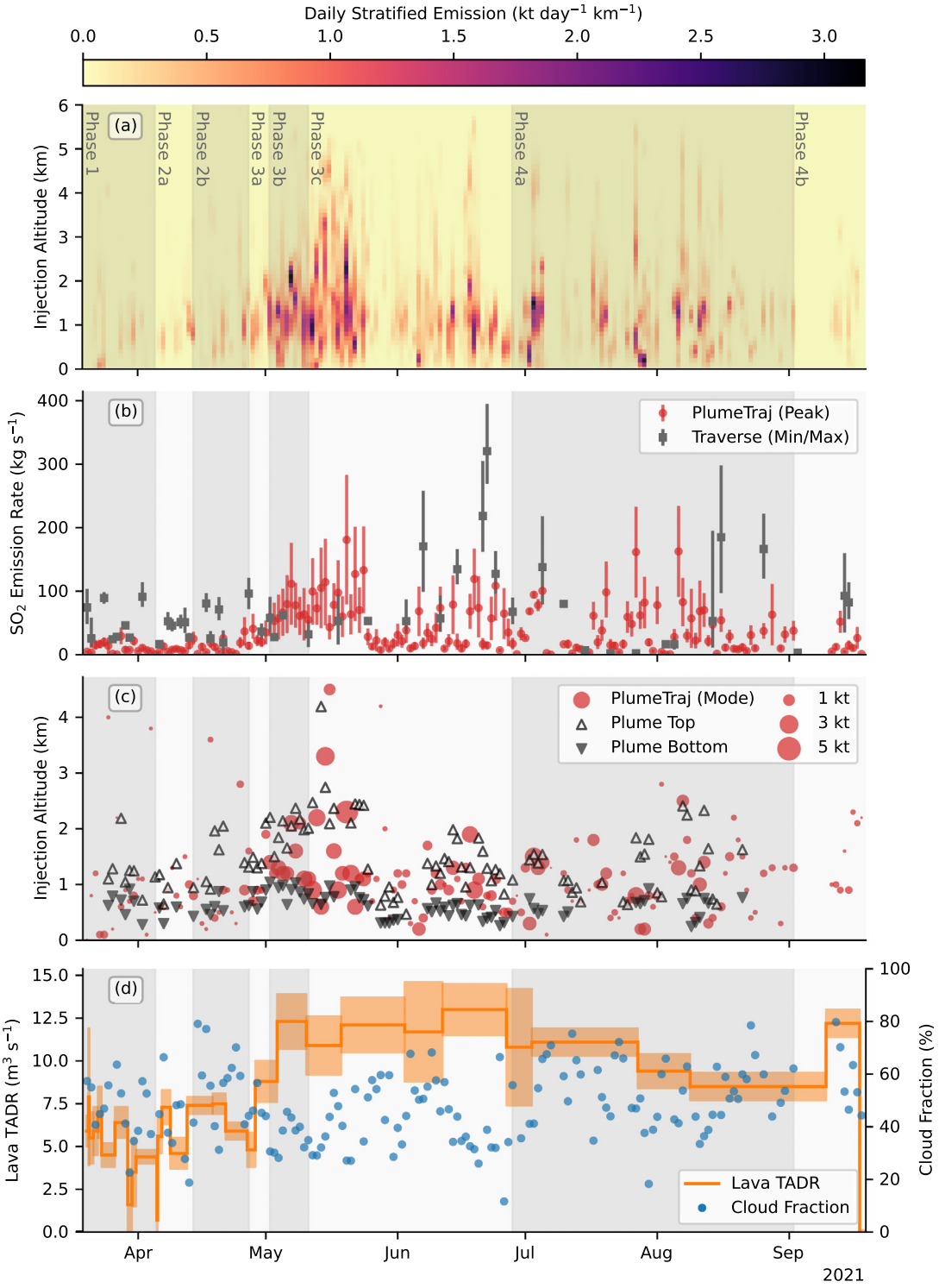

Fig. 4. PlumeTraj derived daily SO_2 emissions from Fagradalsfjall showing (a) the daily total stratified SO_2 emission, (b) daily PlumeTraj peak emission rate (red circles, bars give uncertainty) and mean traverse emission rates (grey squares, bars give range of values), (c) the daily PlumeTraj injection altitudes with the most mass injected (red circles, sized by total emitted SO_2 each day) and camera plume bottom and top heights (grey and white triangles), and (d) lava TDAR (orange line, shaded region gives uncertainty) and the mean cloud fraction of plume pixels (blue circles). Grey shaded regions give the eruption phases from Barsotti et al. (2023).

4.2. Comparison with ground-based measurements

There is good agreement between the PlumeTraj injection altitudes and those from the ground-based cameras throughout (Fig. 4a and 4c). There are some outlying points with very high injection altitudes, however these are very low mass and due to PlumeTraj picking up some noise in the region on days without a substantial plume from the volcano. Throughout the second half of Phase 3c and through Phase 4a there are some emissions assigned to high altitude, typically around 4 km (Fig. 4a). This is not reflected in the camera data and inspection of these days reveals that these higher emissions are due to trajectories taking unrealistic paths back to the volcano. Attempts to correct these were not successful without applying arbitrary altitude limits on the anal-

Table 1
Emission rates from traverse and PlumeTraj for the different eruption stages.

Eruption Phase	Traverse Emission Rate ($kg{\cdot}s^{-1}$)		PlumeTraj Emission Rate ($kg{\cdot}s^{-1}$)	
	Mean (± err)	Standard Deviation	Mean (± err)	Standard Deviation
1	48 (± 6)	31	10 (± 5)	8
2a	40 (± 5)	17	9 (± 4)	7
2b	50 (± 13)	30	13 (± 6)	10
3a	57 (± 14)	35	32 (± 16)	15
3b	54 (± 13)	13	68 (± 37)	17
3c	125 (± 19)	101	52 (± 27)	41
4a	96 (± 21)	79	37 (± 15)	37
4b	71 (± 8)	55	19 (± 8)	16

ysis, which were not seen as a practical solution. As most of the plume mass is returning to the correct altitude (Fig. 4c) this is seen as a minor issue in the overall analysis, but it does show that care must be taken when assessing the results.

The comparison between the PlumeTraj and traverse emission rates is more complicated (Fig. 4b). Table 1 gives an overview of the traverse and PlumeTraj measurements for each phase. In Phases 1 and 2, the traverse emission rates are typically higher than from PlumeTraj, but the agreement improves greatly in Phase 3 where the emission rates and injection altitudes increase. In Phase 4a, both PlumeTraj and the traverses show both very high and very low emission rates, depending on whether they capture an "on" or "off" phase that day, but with comparable magnitudes. Finally, in Phase 4b the PlumeTraj emission rates once again are lower than the traverses.

Assuming the maximum measured emission rate measured each day is representative of that day, then the total emitted SO_2 for the eruption is 520 (± 250) kt. This is at the lower bound of the estimate from the ground-based measurements of 967 (± 538) kt (Barsotti et al., 2023). The uncertainty on the PlumeTraj emission rate is calculated using the minimum and maximum uncertainty limits for each day. This highlights that, although the two values are just within uncertainty of one another, PlumeTraj is systematically underestimating the emission rate with respect to the traverse measurements, apart from the heightened activity in May.

The lava TADR also varies throughout the eruption (Fig. 4d). It is low (~5 $m^3{\cdot}s^{-1}$) in Phases 1 and 2, increases significantly in Phase 3 to ~12 $m^3{\cdot}s^{-1}$, gradually decreases throughout Phase 4 and shows a final burst near the end of the eruption, at which point it ceases. The uptick in TADR in Phase 3 is coincident with the observed increase in SO_2 emission rate from PlumeTraj, while a slight decrease is seen into Phase 4 as the activity shifted to more pulsatory, however the drop in SO_2 emission rate is larger than the relative decrease in TADR.

The cloud fraction also varies throughout the eruption without any clear seasonal trend, typically remaining between 30% and 80%. There is no clear correlation between cloud fraction and measured emission rate, suggesting that variations in observed emissions are real and not driven by meteorological conditions.

Finally, at high latitudes there is a seasonal variation in the available solar UV light used for the SO_2 retrieval, leading to an increase in noise during the local winter months. To test if this could be responsible for the variation in emission rate seen, a region at the same latitude but offset to avoid the SO_2 emission throughout the eruption was investigated (60°N < latitude < 60°N, 60°W < longitude < 55°W). No significant variation in the variability in VCDs was seen across the eruption timeline, though a significant increase in noise is seen prior to and after the activity (Fig. S2). This highlights that the timing of this eruption was fortunate to allow for robust satellite and ground-based UV observations.

The cause for the discrepancy between the traverse and PlumeTraj emission rates was investigated by assessing links between the emission rates on days where both traverses and TROPOMI measurements are available. The results of this are shown in Fig. 5, with the points coloured by the mean cloud fraction, mass-modal injection altitude (the altitude at which the most mass was injected on that day) and the eruption phase. Note that the two lowest traverse points are not visible on the bottom plots as these have differences of 570% and 7100%, so they are not shown for clarity. Ignoring these two points, the mean percentage difference between traverses and PlumeTraj is −49%, with a mean uncertainty of ± 61%. The y-uncertainties on plots d, e and f are calculated by combining the uncertainties in both PlumeTraj and traverse emission rates.

Two rough populations in the emission rates can be seen, with one roughly following the y = x line (within uncertainty range) and the other with TROPOMI emission rates underestimating those from traverses. There is no single clear control on the disparity between emission rates, though typically TROPOMI is underestimating the emission rate with higher cloud fraction and lower altitude plumes. There is also some variation between phases, with TROPOMI emission rates in Phases 1, 2 and 4b systematically underestimated. In Phase 3 there is generally good agreement between the measurements, but into Phases 4 there is a large scatter in points, with both over- and underestimation for each method compared to the other. There is one day on which PlumeTraj greatly exceeds the traverse-based emission rate (27th July). On this day, the PlumeTraj emission rates drop suddenly after 09:00 to zero, capturing the "turning off" of the activity from the vent. The traverse measurement for this day was taken at 12:40, after the shut off, and so measures a much lower emission rate.

The interaction between the plume and cloud depends on their relative altitudes. There is a measure of the cloud height for each pixel available within the operational TROPOMI product, however the precision of this is a function of the cloud cover within that pixel (it is more accurate when there is more cloud present). We compute an effective cloud height as:

$$H^*_{cloud} = (1 - CF) \cdot H_{surf} + CF \cdot H_{cloud} \quad (1)$$

where H^*_{cloud} is the effective cloud height, CF is the cloud fraction (0–1), H_{surf} is the ground surface height, and H_{cloud} is the cloud altitude. All height values are in km above sea level. Using this, we can compute the height difference between the plume and meteorological cloud, ΔH, as:

$$\Delta H = H_{plume} - H^*_{cloud} \quad (2)$$

This value was calculated for all plume pixels throughout the eruption. Fig. 6 displays the results, showing the distribution of ΔH values each day in 0.1 km bins. These results show that there was not a significant change in ΔH throughout the eruption, either from seasonal changes or eruption phases. The peak value for the total pixel count (Fig. 6b) is 0.95 km and there is a jump in total pixel count at 0 km.

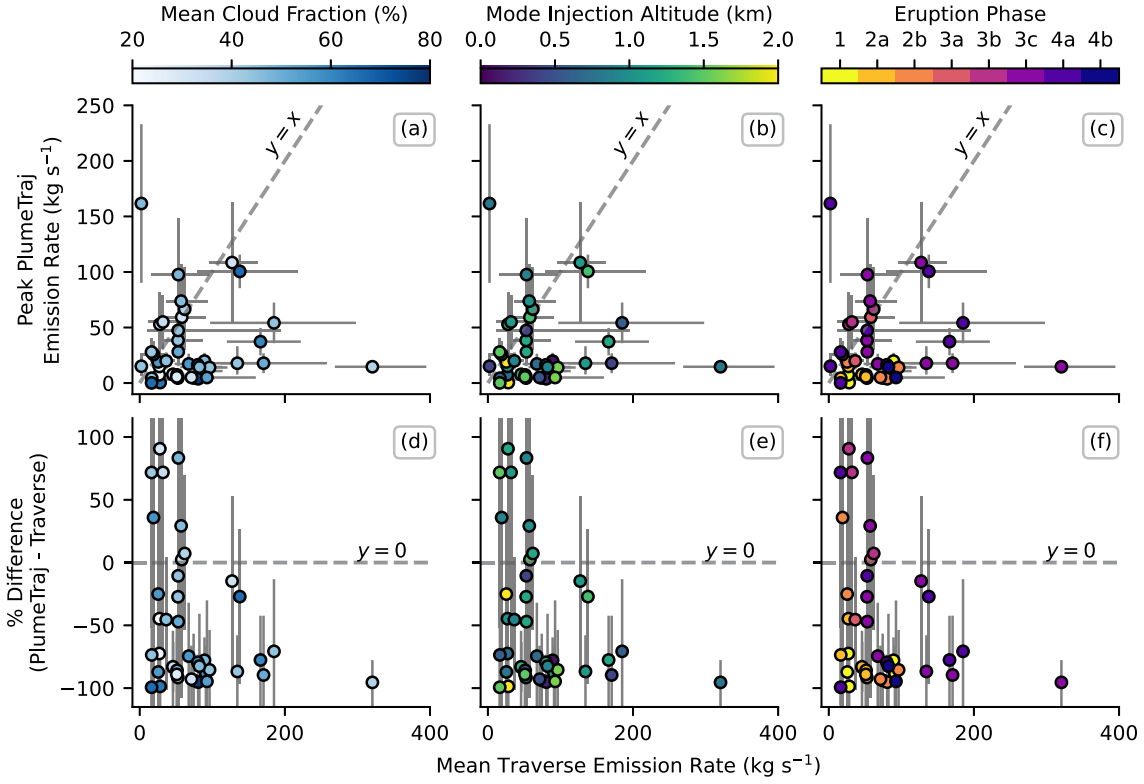

Fig. 5. Comparison between traverse and TROPOMI/PlumeTraj emission rates (top row) and percentage difference from the traverse measurements (bottom row), coloured by (a and d) average cloud fraction of plume pixels, (b and e) mass-modal injection altitude, and (c and f) the eruption phase. Vertical bars give uncertainty estimates on the PlumeTraj emission rates, while horizontal bars give the range of values measured by traverses on that day. Note the y-scale on plots d, e and f has been cropped for clarity.

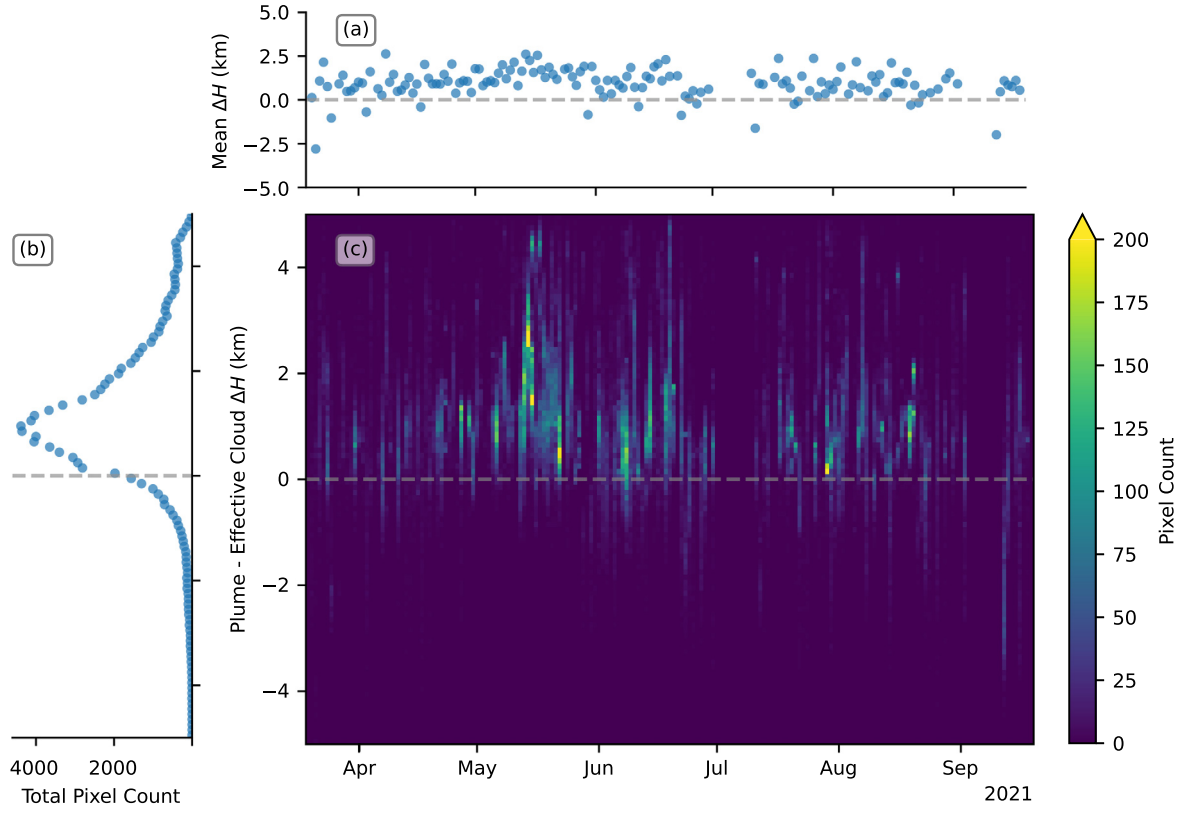

Fig. 6. The height difference between the plume and meteorological cloud, ΔH, calculated as plume altitude minus the effective cloud altitude. (a) the mean ΔH value for each day, (b) the total number of pixels (per 100 m of ΔH) throughout the entire eruption and (c) the number of pixels with given ΔH values (per 100 m of ΔH) per day of the eruption.

These results show that the plume is being detected favourably above the cloud, either due to a lack of sensitivity to plume pixels below the cloud, the fact that the plume is naturally more buoyant than meteorological cloud (due to the thermal energy imparted by the eruption), or a mixture of the two.

5. Discussion

5.1. Comparison with ground-based measurements

There are distinct changes in the emission rates and injection altitudes calculated with PlumeTraj that correlate with the observed phases in the eruption determined from the observations on the ground. Periods of low and high activity can be easily distinguished from the PlumeTraj results, while the change to episodic activity into Phase 4 results in a clear change in the emission signal.

Overall, the agreement between the ground-based observations and PlumeTraj is good, though PlumeTraj does underestimate the emission rates compared to the mobileDOAS measurements during periods of less intense activity. This is not surprising, as we would expect such emissions to be on the edge of detectability due to the relatively low concentration of SO_2, low altitude of emission and high cloud cover in the region. Another point to consider when comparing traverse- and satellite-derived emission rates is that traverses measure the minutes-scale instantaneous emission rate at the time of measurement (the length of time required to complete the traverse), whereas the satellite measurement is an average over a given time window (depending on the model time step and pixel sizes). This means that short-term variation in emission rate may result in very low or high emission rates from a traverse, whereas these will be smoothed to a mean value in satellite measurements. This is why traverses were repeated multiple times on each measurement day. This is also reflected in the discrepancy between traverses and PlumeTraj during the episodic activity, where either the PlumeTraj or traverse measurement can be higher than the other depending on whether they capture an “on” or “off” phase in the emissions at the time of measurement.

The uncertainty in the emission rate introduced by the GFS data is difficult to assess quantitatively. Traverses require a measurement of wind speed to calculate the emission rate from the measured plume cross-section, in this case taken from the HARMONIE model (Bengtsson et al., 2017; Icelandic Met Office, 2015). The uncertainties on this wind speed are transferred directly to the measured emission rate. With PlumeTraj, however, the emission rate is calculated by summing the mass returning to the vent within a given time frame and dividing by the length of that time frame, so the uncertainties in the wind speed are not directly correlated to the emission rate. As the total mass is conserved, when using the peak emission rate, the uncertainties in the wind speed should not have a dramatic impact on the emission rate value, but rather the exact time at which it is measured. Care should be taken when inspecting time-variations in emission rate from older plumes, as there is more time for inaccuracies in the meteorological data to contribute to the arrival time.

Analysing the relationship between the TROPOMI and traverse emission rates, the best agreement is found when the emissions are steady, with a higher injection altitude and with minimal cloud cover. During the episodic activity (Phase 4a) the emission rate measured by either method depends strongly on whether an on- or off-phase in the activity is captured. There are also significant sources of uncertainty for ground-based measurements, including the wind speed used, radiative transfer issues (including light dilution and multiple scattering within the plume) and geometrical corrections that must be applied to calculate the emission rate. It is worth noting that no corrections for scattering below the plume were made for the traverse measurements, an effect which tends to lead to a systematic underestimation of the emission rate. The plume was typically low altitude, low concentration and optically thin, which will minimise this impact. The sampling frequency will also impose uncertainties when the emission rate is highly variable, as making traverse measurements is very labour intensive and cannot be practically applied continuously. As with PlumeTraj, the best results will be found for steady emission under clear skies, though traverses are more sensitive to lower altitude plumes instead of higher ones.

The relationship between the plume and cloud altitudes shows that the plume is being detected favourably above the cloud. There is a small jump in values at $\Delta H = 0$, suggesting that some pixels lower than the cloud level are not being detected due to being obscured, however it seems that most of the plume is being injected above the cloud level and is staying there. It is worth noting that, although the precision on the cloud altitude is high (typically $<$ 0.1 km here), there are large systematic errors that can affect these measurements (Compernolle et al., 2021). Since the cloud fraction and altitude are key parameters in the calculation of the air mass factor (AMF) to convert the measured slant column density (SCD) to the VCD, this means that the true uncertainty on the corrected VCD due to clouds is likely to be much larger than currently reported. This is an area that requires future work.

The agreement between the injection altitudes measured by PlumeTraj and the visible cameras is better, with the range of altitudes measured during a day from the visible cameras generally covering the observed altitudes of emission from PlumeTraj. There are days with much higher (up to 4-5 km) and very low (down to ground level) emissions which likely reflects the limitations of the meteorological model used. The back-trajectories also do not account for any diffusion of the plume, so plume edges may return at incorrect altitudes if this is a major factor. Additionally, the meteorological data has a relatively coarse spatial resolution (0.25°), so using a finer scale model may help to correct these anomalous results. However, the fact that these results are generally in agreement with the ground-measured altitude shows that PlumeTraj can produce useful information even when the absolute emission rates are not accurate.

5.2. Volcanological implications

The calculated SO_2 emission rates show that the emission behaviour was very variable throughout the eruption, with three periods of increased emission, both in terms of measured emitted SO_2 and injection altitude (Fig. 4a). This is partially missed by the traverses due to the sparser nature of the measurements but is reflected in the camera-derived plume altitudes. The first period (in May) is the most sustained, while the following two (in June and mid-July to mid-August) are during the episodic activity.

The initial magma sulphur content can be estimated by combining the measured SO_2 emission rate with the lava TADR. We converted the reported lava volume effusion rates reported by Pedersen et al. (2022a) (and shown in Fig. 4d) to a mass effusion rate by multiplying by a typical Icelandic density of 2700 $kg{\cdot}m^{-3}$ (Hartley and Maclennan, 2018). The results are shown in Fig. 7, alongside a measure of the sulphur content determined from melt inclusions sampled during the early stages of the eruption (Halldórsson et al., 2022).

The calculated sulphur content is initially lower than those from the melt inclusions (except two data points corresponding to very low lava emission rates), but this increases dramatically in May when the SO_2 emission first increases. There is a further peak at the beginning of August during the third pulse in SO_2 emission, however no significant increase is seen during the second pulse in June.

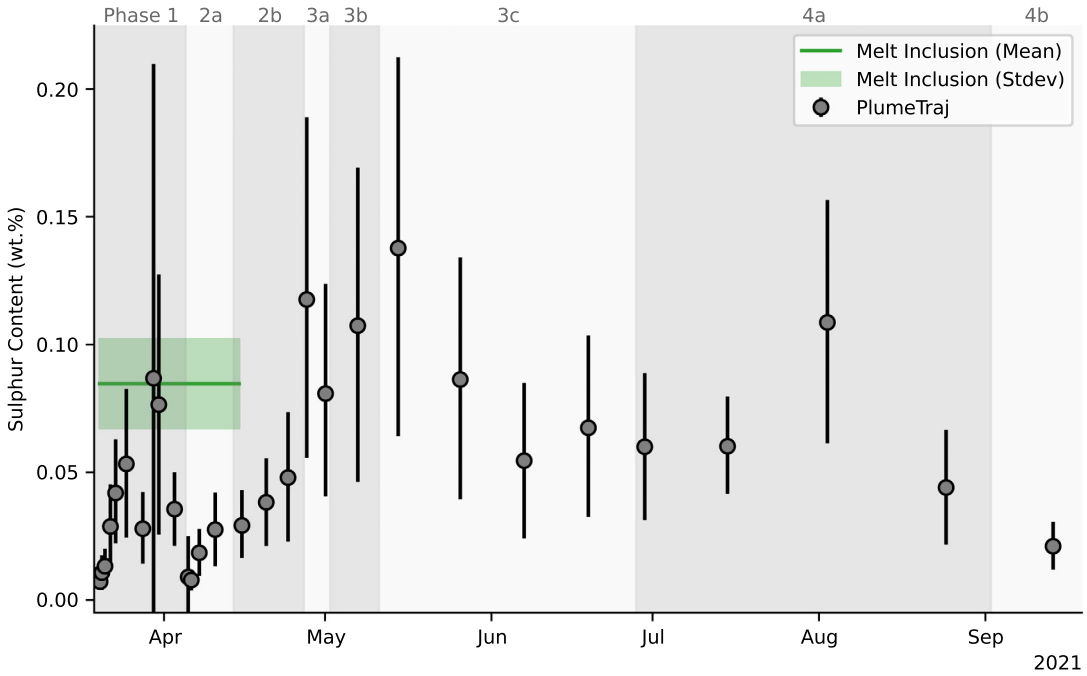

Fig. 7. Initial magma sulphur content, calculated from PlumeTraj SO_2 emission rates and reported lava TADR. Also shown is the sulphur content from melt inclusions from the beginning of the eruption (Halldórsson et al., 2022). The time of each point is the mid-point of the time window used to calculate the lava effusion rate.

It is not immediately obvious what causes the peaks in emission seen. The first pulse in May corresponds to a dramatic increase in the mass eruption rate and higher altitude, sustained plumes. The second pulse is associated with a slight increase in the lava TADR, but the third is during the steady decline in lava emission towards the end of the eruption. This is reflected in the calculated magma sulphur contents, with peaks in pulses 1 and 3, but not a clear increase in pulse 2. This suggests that the magma source had a time varying composition, highlighting a need for further geochemical analysis of the lava throughout the eruption.

6. Conclusions

In this paper, altitude- and time-resolved SO_2 emissions from the 2021 eruption of Fagradalsfjall are quantified by analysing SO_2 imagery from TROPOMI with the PlumeTraj back-trajectory analysis toolkit. The closest agreement is found when comparing with emission rates measured by mobileDOAS traverse and plume injection altitudes measured by calibrated visible cameras, though emission rates during periods of lower activity were generally lower from PlumeTraj than the traverses.

Changes in the surface activity observed at Fagradalsfjall correlate well with changes in the observed emission rate and altitude. Periods of higher eruption intensity (e.g. Phase 3) are reflected by higher emission rates and higher injection altitudes, while the change to episodic emissions in Phase 4a is clearly reflected in the two populations of emission rate values observed from day to day. This clearly demonstrates that the combination of TROPOMI and PlumeTraj is a useful tool for monitoring volcanic SO_2 emissions from relatively low intensity effusive eruptions. Care must be taken however, as TROPOMI/PlumeTraj tends to underestimate the emission rate when the cloud fraction is high and if the injection altitude is low. The role of the cloud fraction and cloud height are large sources of uncertainty, requiring future work to improve this.

Three distinct pulses in stronger and higher altitude SO_2 emission are seen, which are less clear in the sparser traverse measurements. These do not always correspond to increases in the lava effusion rate, suggesting a time evolving volatile content of the magma. This requires further investigation and comparison with chemical analyses of samples taken throughout the eruption to better understand the driving mechanism behind this.

There are some results that appear to be anomalous, specifically the higher altitude (roughly 4 km) emissions seen in Phase 4a (Fig. 4a). These are most likely due to issues with the trajectory model and/or the meteorological data used, as the resolution of the data is low (0.25°) and the behaviour of such models close to the ground can be poor when topography is not well resolved. This is a limit of the global-scale data used, especially for plumes so close to the ground. This could be improved in the future by incorporating finer resolution meteorological data into PlumeTraj, which is the subject of ongoing work.

PlumeTraj can measure the SO_2 emission rates on most days throughout the eruption and does not measure any emissions before or after the eruption, or during pauses in activity, making it a useful tool to determine activity start and end dates for unmonitored volcanoes globally. The 2021 eruption of the Fagradalsfjall volcanic system presented an ideal test for PlumeTraj, as the high latitude, low plume altitude, high cloud cover, low SO_2 concentrations and dynamic eruption style made this a particularly challenging application. For other volcanoes at lower latitude and with typically less cloud cover we would expect PlumeTraj to perform even better.

The required data for PlumeTraj are freely available in near real-time and the processing can be easily automated, demonstrating the power of PlumeTraj to provide 24-hour monitoring for future effusive eruptions. This is especially useful for volcanoes without the dedicated infrastructure for such measurements, for hard to access volcanoes, or for filling in gaps in ground-based monitoring time-series to improve existing coverage.

CRediT authorship contribution statement

Ben Esse: Writing – review & editing, Writing – original draft, Visualization, Validation, Software, Methodology, Investigation, Formal analysis, Data curation, Conceptualization. **Mike Burton:** Writing – review & editing, Supervision, Project administration, Methodology, Funding acquisition. **Catherine Hayer:** Writing – review & editing, Software, Methodology. **Melissa Anne Pfeffer:**

Writing – review & editing, Investigation. **Sara Barsotti:** Writing – review & editing, Investigation. **Nicolas Theys:** Writing – review & editing, Data curation. **Talfan Barnie:** Writing – review & editing, Investigation. **Manuel Titos:** Writing – review & editing, Investigation.

Declaration of competing interest

The authors declare that they have no known competing financial interests or personal relationships that could have appeared to influence the work reported in this paper.

Data availability

The TROPOMI COBRA SO_2 data used in this study can be accessed from the BIRA-IASB software distribution site (https://distributions.aeronomie.be/). The GFS meteorological data can be accessed from the NOAA data archive (https://www.ready.noaa.gov/data/archives/gfs0p25/). All satellite SO_2 emission data presented in this paper can be accessed here: https://www.doi.org/10.6084/m9.figshare.22303435. Traverse and plume height data were taken and analysed by IMO and are available upon request.

Acknowledgements

This work was supported by the UK Natural Environment Research Council (NERC) funded V-PLUS (NE/S004106/1) and DisEqm (NE/N018575/1) projects, and the Centre for Observation and Modelling of Earthquakes, Volcanoes, and Tectonics (COMET). The TROPOMI COBRA SO_2 product was developed under ESA S5P MPC (grant no. 4000117151/16/I-LG), ESA S5P PAL (https://data-portal.s5p-pal.com/), Belgium Prodex TRACE-S5P (grant no. PEA 5 4000105598) projects. The TROPOMI COBRA SO_2 product can be obtained through the S5P PAL data portal (https://data-portal.s5p-pal.com/).

Appendix A. Supplementary material

Supplementary material related to this article can be found online at https://doi.org/10.1016/j.epsl.2023.118325.

References

Aiuppa, A., Moretti, R., Federico, C., Giudice, G., Gurrieri, S., Liuzzo, M., Papale, P., Shinohara, H., Valenza, M., 2007. Forecasting Etna eruptions by real-time observation of volcanic gas composition. Geology 35 (12), 1115–1118. https://doi.org/10.1130/G24149A.1.

Barnie, T., Hjörvar, T., Titos, M., Sigurðsson, E.M., Pálsson, S.K., Bergsson, B., Ingvarsson, Þ., Pfeffer, M.A., Barsotti, S., Arason, Þ., Þorvaldsson, V.S., von Löwis of Menar, S., Oddsson, B., 2023. Volcanic plume height monitoring using calibrated web cameras at the Icelandic Meteorological Office: system overview and first application during the 2021 Fagradalsfjall eruption. J. Appl. Volcanol. 12 (1), 4. https://doi.org/10.1186/s13617-023-00130-9.

Barsotti, S., 2020. Probabilistic hazard maps for operational use: the case of SO_2 air pollution during the Holuhraun eruption (Bárðarbunga, Iceland) in 2014–2015. Bull. Volcanol. 82 (7), 56. https://doi.org/10.1007/s00445-020-01395-3.

Barsotti, S., Parks, M.M., Pfeffer, M.A., Óladóttir, B.A., Barnie, T., Titos, M.M., Jónsdóttir, K., Pedersen, G.B.M., Hjartardóttir, Á.R., Stefansdóttir, G., Johannsson, T., Arason, Þ., Gudmundsson, M.T., Oddsson, B., Þrastarson, R.H., Ófeigsson, B.G., Vogfjörd, K., Geirsson, H., Hjörvar, T., et al., 2023. The eruption in Fagradalsfjall (2021, Iceland): how the operational monitoring and the volcanic hazard assessment contributed to its safe access. Nat. Hazards. https://doi.org/10.1007/s11069-022-05798-7.

Bengtsson, L., Andrae, U., Aspelien, T., Batrak, Y., Calvo, J., Rooy, W. de, Gleeson, E., Hansen-Sass, B., Homleid, M., Hortal, M., Ivarsson, K.-I., Lenderink, G., Niemelä, S., Nielsen, K.P., Onvlee, J., Rontu, L., Samuelsson, P., Muñoz, D.S., Subias, A., et al., 2017. The HARMONIE–AROME model configuration in the ALADIN–HIRLAM NWP system. Monthly Weather Review 145 (5), 1919–1935. https://doi.org/10.1175/MWR-D-16-0417.1.

Bindeman, I.N., Deegan, F.M., Troll, V.R., Thordarson, T., Höskuldsson, Á., Moreland, W.M., Zorn, E.U., Shevchenko, A.V., Walter, T.R., 2022. Diverse mantle components with invariant oxygen isotopes in the 2021 Fagradalsfjall eruption, Iceland. Nat. Commun. 13 (1), 3737. https://doi.org/10.1038/s41467-022-31348-7.

Burton, M., Hayer, C., Miller, C., Christenson, B., 2021. Insights into the 9 December 2019 eruption of Whakaari/White Island from analysis of TROPOMI SO_2 imagery. Sci. Adv. 7 (25). https://doi.org/10.1126/sciadv.abg1218.

Carlsen, H.K., Ilyinskaya, E., Baxter, P.J., Schmidt, A., Thorsteinsson, T., Pfeffer, M.A., Barsotti, S., Dominici, F., Finnbjornsdottir, R.G., Jóhannsson, T., Aspelund, T., Gislason, T., Valdimarsdóttir, U., Briem, H., Gudnason, T., 2021. Increased respiratory morbidity associated with exposure to a mature volcanic plume from a large Icelandic fissure eruption. Nat. Commun. 12 (1), 1. https://doi.org/10.1038/s41467-021-22432-5.

Carn, S.A., Fioletov, V.E., McLinden, C.A., Li, C., Krotkov, N.A., 2017. A decade of global volcanic SO_2 emissions measured from space. Sci. Rep. 7, 44095. https://doi.org/10.1038/srep44095.

Compernolle, S., Argyrouli, A., Lutz, R., Sneep, M., Lambert, J.-C., Fjæraa, A.M., Hubert, D., Keppens, A., Loyola, D., O'Connor, E., Romahn, F., Stammes, P., Verhoelst, T., Wang, P., 2021. Validation of the Sentinel-5 Precursor TROPOMI cloud data with Cloudnet, Aura OMI O_2–O_2, MODIS, and Suomi-NPP VIIRS. Atmos. Meas. Tech. 14 (3), 2451–2476. https://doi.org/10.5194/amt-14-2451-2021.

Esse, B., Burton, M., Hayer, C., Contreras-Arratia, R., Christopher, T., Joseph, E.P., Varnam, M., Johnson, C., 2023. SO_2 emissions during the 2021 eruption of La Soufrière St. Vincent, revealed with back-trajectory analysis of TROPOMI imagery. Geol. Soc. (Lond.) Spec. Publ. 539 (1). https://doi.org/10.1144/SP539-2022-77.

Flóvenz, Ó.G., Wang, R., Hersir, G.P., Dahm, T., Hainzl, S., Vassileva, M., Drouin, V., Heimann, S., Isken, M.P., Gudnason, E.Á., Ágústsson, K., Ágústsdóttir, T., Horálek, J., Motagh, M., Walter, T.R., Rivalta, E., Jousset, P., Krawczyk, C.M., Milkereit, C., 2022. Cyclical geothermal unrest as a precursor to Iceland's 2021 Fagradalsfjall eruption. Nat. Geosci. 15 (5), 397–404. https://doi.org/10.1038/s41561-022-00930-5.

Global Volcanism Program, 2021. Report on Krysuvik-Trolladyngja (Iceland). (46:5; Bulletin of the Global Volcanism Project). https://doi.org/10.5479/si.GVP.BGVN202105-371030.

Halldórsson, S.A., Marshall, E.W., Caracciolo, A., Matthews, S., Bali, E., Rasmussen, M.B., Ranta, E., Robin, J.G., Guðfinnsson, G.H., Sigmarsson, O., Maclennan, J., Jackson, M.G., Whitehouse, M.J., Jeon, H., van der Meer, Q.H.A., Mibei, G.K., Kalliokoski, M.H., Repczynska, M.M., Rúnarsdóttir, R.H., et al., 2022. Rapid shifting of a deep magmatic source at Fagradalsfjall volcano, Iceland. Nature 609 (7927), 7927. https://doi.org/10.1038/s41586-022-04981-x.

Hartley, M., Maclennan, J., 2018. Magmatic densities control erupted volumes in Icelandic volcanic systems. Front. Earth Sci. 6. https://www.frontiersin.org/articles/10.3389/feart.2018.00029.

Hayer, C., Burton, M., Ferrazzini, V., Esse, B., Di Muro, A., 2023. Unusually high SO_2 emissions and plume height from Piton de la Fournaise volcano during the April 2020 eruption. Bull. Volcanol. 85 (4), 21. https://doi.org/10.1007/s00445-023-01628-1.

Hayer, C., Wadge, G., Edmonds, M., Christopher, T., 2016. Sensitivity of OMI SO_2 measurements to variable eruptive behaviour at Soufrière Hills Volcano, Montserrat. J. Volcanol. Geotherm. Res. 312, 1–10. https://doi.org/10.1016/j.jvolgeores.2016.01.014.

Icelandic Met Office, 2015. HARMONIE - numerical weather prediction model. https://en.vedur.is/weather/articles/nr/3232. (Accessed 3 July 2023).

Ilyinskaya, E., Schmidt, A., Mather, T.A., Pope, F.D., Witham, C., Baxter, P., Jóhannsson, T., Pfeffer, M., Barsotti, S., Singh, A., Sanderson, P., Bergsson, B., McCormick Kilbride, B., Donovan, A., Peters, N., Oppenheimer, C., Edmonds, M., 2017. Understanding the environmental impacts of large fissure eruptions: aerosol and gas emissions from the 2014–2015 Holuhraun eruption (Iceland). Earth Planet. Sci. Lett. 472, 309–322. https://doi.org/10.1016/j.epsl.2017.05.025.

Kristiansen, N.I., Stohl, A., Prata, A.J., Richter, A., Eckhardt, S., Seibert, P., Hoffmann, A., Ritter, C., Bitar, L., Duck, T.J., Stebel, K., 2010. Remote sensing and inverse transport modeling of the Kasatochi eruption sulfur dioxide cloud. J. Geophys. Res., Atmos. 115 (D2). https://doi.org/10.1029/2009JD013286.

Lowenstern, J.B., Wallace, K., Barsotti, S., Sandri, L., Stovall, W., Bernard, B., Privitera, E., Komorowski, J.-C., Fournier, N., Balagizi, C., Garaebiti, E., 2022. Guidelines for volcano-observatory operations during crises: recommendations from the 2019 volcano observatory best practices meeting. J. Appl. Volcanol. 11 (1), 3. https://doi.org/10.1186/s13617-021-00112-9.

Óladóttir, B.A., 2022. Fagradalsfjall. In: Óladóttir, B.A., Larsen, G., Guðmundsson, M.T. (Eds.), Catalogue of Icelandic Volcanoes. IMO, UI and CPD-NCIP. https://icelandicvolcanos.is/?volcano=FAG#.

Oppenheimer, C., Scaillet, B., Martin, R.S., 2011. Sulfur degassing from volcanoes: source conditions, surveillance, plume chemistry and Earth system impacts. Rev. Mineral. Geochem. 73 (1), 363–421. https://doi.org/10.2138/rmg.2011.73.13.

Pallister, J., Papale, P., Eichelberger, J., Newhall, C., Mandeville, C., Nakada, S., Marzocchi, W., Loughlin, S., Jolly, G., Ewert, J., Selva, J., 2019. Volcano observatory best practices (VOBP) workshops—a summary of findings and best-practice recommendations. J. Appl. Volcanol. 8 (1), 2. https://doi.org/10.1186/s13617-019-0082-8.

Pardini, F., Burton, M., de' Michieli Vitturi, M., Corradini, S., Salerno, G., Merucci, L., Di Grazia, G., 2017. Retrieval and intercomparison of volcanic SO_2 injection height and eruption time from satellite maps and ground-based observations. J. Volcanol. Geotherm. Res. 331, 79–91. https://doi.org/10.1016/j.jvolgeores.2016.12.008.

Pedersen, G.B.M., Belart, J.M.C., Óskarsson, B.V., Gudmundsson, M.T., Gies, N., Högnadóttir, T., Hjartardóttir, Á.R., Pinel, V., Berthier, E., Dürig, T., Reynolds, H.I., Hamilton, C.W., Valsson, G., Einarsson, P., Ben-Yehosua, D., Gunnarsson, A., Oddsson, B., 2022a. Volume, effusion rate, and lava transport during the 2021 Fagradalsfjall eruption: results from near real-time photogrammetric monitoring. Geophys. Res. Lett. 49 (13), e2021GL097125. https://doi.org/10.1029/2021GL097125.

Pedersen, G.B.M., Pfeffer, M.A., Barsotti, S., Tarquini, S., de' Michieli Vitturi, M., Óladóttir, B., Þrasstarson, R.H., 2022b. Lava flow hazard modelling during the 2021 Fagradalsfjall eruption, Iceland: applications of MrLavaLoba. Nat. Hazards Earth Syst. Sci. Discuss. https://doi.org/10.5194/nhess-2022-166. Preprint.

Pfeffer, M.A., Bergsson, B., Barsotti, S., Stefánsdóttir, G., Galle, B., Arellano, S., Conde, V., Donovan, A., Ilyinskaya, E., Burton, M., Aiuppa, A., Whitty, R.C.W., Simmons, I.C., Arason, Þ., Jónasdóttir, E.B., Keller, N.S., Yeo, R.F., Arngrímsson, H., Jóhannsson, Þ., et al., 2018. Ground-based measurements of the 2014–2015 Holuhraun volcanic cloud (Iceland). Geosciences 8 (1), 1. https://doi.org/10.3390/geosciences8010029.

Queißer, M., Burton, M., Theys, N., Pardini, F., Salerno, G., Caltabiano, T., Varnam, M., Esse, B., Kazahaya, R., 2019. TROPOMI enables high resolution SO_2 flux observations from Mt. Etna, Italy, and beyond. Sci. Rep. 9 (1), 957. https://doi.org/10.1038/s41598-018-37807-w.

Robock, A., 2000. Volcanic eruptions and climate. Rev. Geophys. 38 (2), 191–219. https://doi.org/10.1029/1998RG000054.

Sæmundsson, K., Sigurgeirsson, M.Á., Friðleifsson, G.Ó., 2020. Geology and structure of the Reykjanes volcanic system, Iceland. J. Volcanol. Geotherm. Res. 391, 106501. https://doi.org/10.1016/j.jvolgeores.2018.11.022.

Salerno, G.G., Burton, M., Di Grazia, G., Caltabiano, T., Oppenheimer, C., 2018. Coupling between magmatic degassing and volcanic tremor in basaltic volcanism. Front. Earth Sci. 6. https://doi.org/10.3389/feart.2018.00157.

Sigmundsson, F., Parks, M., Hooper, A., Geirsson, H., Vogfjörd, K.S., Drouin, V., Ófeigsson, B.G., Hreinsdóttir, S., Hjaltadóttir, S., Jónsdóttir, K., Einarsson, P., Barsotti, S., Horálek, J., Ágústsdóttir, T., 2022. Deformation and seismicity decline before the 2021 Fagradalsfjall eruption. Nature 1 (6). https://doi.org/10.1038/s41586-022-05083-4.

Sparks, R.S.J., 2003. Forecasting volcanic eruptions. Earth Planet. Sci. Lett. 210 (1–2), 1–15. https://doi.org/10.1016/s0012-821x(03)00124-9.

Tam, E., Miike, R., Labrenz, S., Sutton, A.J., Elias, T., Davis, J., Chen, Y.-L., Tantisira, K., Dockery, D., Avol, E., 2016. Volcanic air pollution over the Island of Hawai'i: emissions, dispersal, and composition. Association with respiratory symptoms and lung function in Hawai'i Island school children | Elsevier Enhanced Reader. Environ. Int. 92–93, 543–552. https://doi.org/10.1016/j.envint.2016.03.025.

Tarquini, S., Favalli, M., Pfeffer, M., De' Michieli Vitturi, M., Barsotti, S., Pedersen, G., Óladóttir, B.A., Jensen, E.H., 2020. Assessing the impact of lava flows during the unrest of Svartsengi volcano in the Reykjanes peninsula, Iceland. In: Proceedings of the Geomorphometry 2020 Conference, Geomorphometry. Perugia, Italy.

Theys, N., Campion, R., Clarisse, L., Brenot, H., van Gent, J., Dils, B., Corradini, S., Merucci, L., Coheur, P.-F., Van Roozendael, M., Hurtmans, D., Clerbaux, C., Tait, S., Ferrucci, F., 2013. Volcanic SO_2 fluxes derived from satellite data: a survey using OMI, GOME-2, IASI and MODIS. Atmos. Chem. Phys. 13 (12), 5945–5968. https://doi.org/10.5194/acp-13-5945-2013.

Theys, N., Fioletov, V., Li, C., De Smedt, I., Lerot, C., McLinden, C., Krotkov, N., Griffin, D., Clarisse, L., Hedelt, P., Loyola, D., Wagner, T., Kumar, V., Innes, A., Ribas, R., Hendrick, F., Vlietinck, J., Brenot, H., Van Roozendael, M., 2021. A sulfur dioxide covariance-based retrieval algorithm (COBRA): application to TROPOMI reveals new emission sources. Atmos. Chem. Phys. 21 (22), 16727–16744. https://doi.org/10.5194/acp-21-16727-2021.

Theys, N., Hedelt, P., De Smedt, I., Lerot, C., Yu, H., Vlietinck, J., Pedergnana, M., Arellano, S., Galle, B., Fernandez, D., Carlito, C.J.M., Barrington, C., Taisne, B., Delgado-Granados, H., Loyola, D., Van Roozendael, M., 2019. Global monitoring of volcanic SO_2 degassing with unprecedented resolution from TROPOMI onboard Sentinel-5 Precursor. Sci. Rep. 9 (1), 1. https://doi.org/10.1038/s41598-019-39279-y.

Thordarson, T., Self, S., 2003. Atmospheric and environmental effects of the 1783–1784 Laki eruption: a review and reassessment. J. Geophys. Res., Atmos. 108 (D1), 7–1-AAC 7-29. https://doi.org/10.1029/2001JD002042.

Veefkind, J.P., Aben, I., McMullan, K., Förster, H., de Vries, J., Otter, G., Claas, J., Eskes, H.J., de Haan, J.F., Kleipool, Q., van Weele, M., Hasekamp, O., Hoogeveen, R., Landgraf, J., Snel, R., Tol, P., Ingmann, P., Voors, R., Kruizinga, B., et al., 2012. TROPOMI on the ESA Sentinel-5 Precursor: a GMES mission for global observations of the atmospheric composition for climate, air quality and ozone layer applications. Remote Sens. Environ. 120, 70–83. https://doi.org/10.1016/j.rse.2011.09.027.

von Glasow, R., Bobrowski, N., Kern, C., 2009. The effects of volcanic eruptions on atmospheric chemistry. Chem. Geol. 263 (1), 131–142. https://doi.org/10.1016/j.chemgeo.2008.08.020.

Whitty, R.C.W., Ilyinskaya, E., Mason, E., Wieser, P.E., Liu, E.J., Schmidt, A., Roberts, T., Pfeffer, M.A., Brooks, B., Mather, T.A., Edmonds, M., Elias, T., Schneider, D.J., Oppenheimer, C., Dybwad, A., Nadeau, P.A., Kern, C., 2020. Spatial and temporal variations in SO_2 and $PM_{2.5}$ levels around Kīlauea Volcano, Hawai'i during 2007–2018. Front. Earth Sci., 8. https://doi.org/10.3389/feart.2020.00036.